DELIVERABLE # 4: GaN Devices

Faculty: Dipankar Saha, Subhabrata Dhar , Subhananda Chakrabati, J Vasi
Researchers & Students: Sreenivas Subramanian, Tarakeshwar C. Patil, A. Mukherjee, A. Ghosh, Prantik Mahajan and S. Subramanian

4.1 Introduction:

There has been a lot of interest worldwide on GaN/AlGaN based devices [1]. The wide bandgap (3.4-6.2 eV), large breakdown field (3 MV/cm), high saturation velocity (10^7 cm.s^{-1}) for electrons, radiation hardness, high two dimensional electron-gas density (~10^{13} cm^{-3}), and high temperature operation make them ideal for high power and high speed devices [2]. GaN/AlGaN based high electron mobility transistors (HEMT), light emitting diodes (LED) and lasers are the most important class of devices in this area for various applications. We have made a focussed effort on the realization of a HEMT for RF applications. The basic HEMT device is grown at TIFR, and fabricated and characterized at IIT-B.

4.2 Goals:

4.2.1 The goal of this effort is to fabricate and characterize the GaN/AlGaN HEMT device. The various transistor parameters *e.g.* threshold voltage (V_{TH}), transconductance (g_m), current unity gain frequency (f_T) etc. are to be extracted.

4.2.1 The successful HEMT fabrication depends on the development of the individual process steps (Ohmic contact, Schottky contact, and controlled, selective and anisotropic etch for GaN/AlGaN) to optimize the HEMT characteristics. The complete process development is also undertaken this year.

4.3 Timelines:

Year 4 (current): We have fabricated and characterized the basic HEMT device. We have successfully developed most of the processes for III-V nano-fabrication.
Year 5: sub-100 nm HEMT fabrication with state-of-the-art characteristics, blue LED fabrication and characterization.

We are right on schedule for this deliverable.

4.4 Progress during last one year:

A substantial progress has been made over the last year, which has led to the realization of the GaN HEMT. All the individual process steps have been characterized for III-V nano-fabrication.

A schematic of the HEMT heterostructure is shown in Fig. 4.1. The heterostructure is grown by MOCVD. The heterostructure contains an undoped AlN layer to reduce

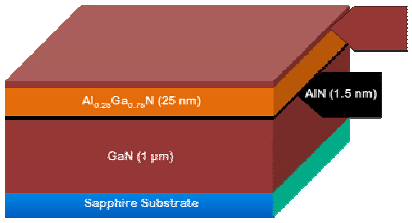

Fig. 4.1 A schematic of the GaN heterostructure

impurity scattering of the 2DEG channel electrons present at AlGaN/GaN interface. The Al concentration is optimized to create enough confinement by appropriate conduction band-offset and minimize interface defects. The device is fabricated in the following steps: (a) recess etching for source and drain, ohmic contact metal deposition and annealing, (b) mesa etching, (c) gate recess etching, and (d) gate metal (Schottky contact) deposition. A schematic of the flow is shown in Fig. 4.2.

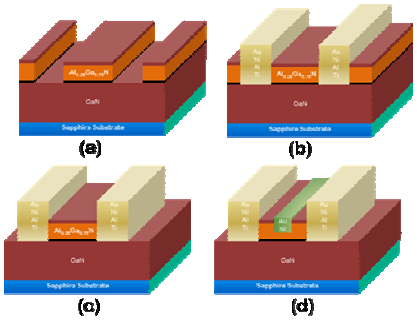

Fig. 4.2 A Schematic of the process flow for HEMT fabrication.

Hence, the process calibrations involved with the device fabrication are: (1) good ohmic contact for source and drain terminals, (2) good Schottky contact for gate terminal, (3) anisotropic and fast etching for mesa, and (4) controlled, anisotropic and selective etching for source/drain and gate terminals. A metal stack of Ti/Al/Ni/Au (20/150/50/125 nm) is used for making ohmic contact. The annealing temperature is varied from 700 – 850 ^{o}C in steps of 25 ^{o}C and conductivity measurements are done. The measured conductivity as a function of annealing temperature is shown in Fig. 4.3. The

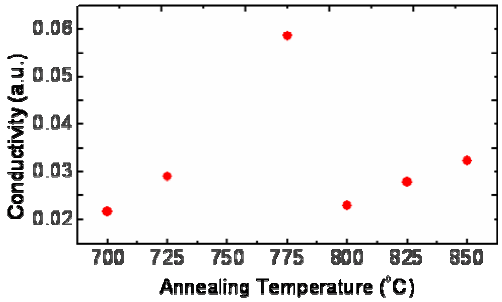

Fig. 4.3 Ohmic contact conductivity as a function of annealing temperature.

minimum contact resistance is measured at 775 ^{o}C, which is used as the annealing temperature for source/drain contacts. The current-voltage (*I-V*) measurement for a typical contact annealed at 775 ^{o}C is shown in Fig. 4.4. A perfect linear *I-V*

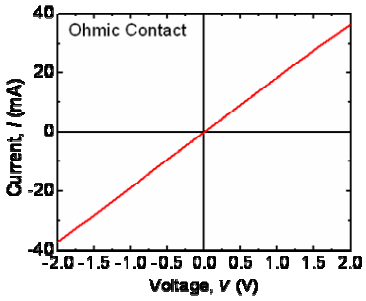

Fig. 4.4 Linear I-V characteristics of an ohmic contact anneal at 775 ^{o}C.

characteristic is measured experimentally. A Ni/Au (10/100 nm) metal stack is used for Schottky contact. The metal deposition is done using e-beam physical vapour deposition technique. The *I-V* characteristics of the Schottky contact is shown in Fig. 4.5. There is a large leakage current in the reverse bias condition due to the background *n*-doping of the GaN nucleation layer. An effort will be made in future two reduce the background doping and

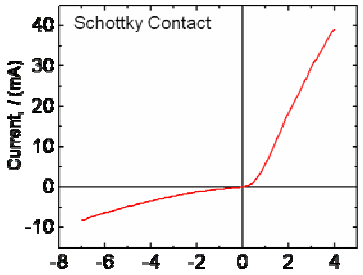

Fig. 4.5 A typical Schottky barrier characteristics.

improve upon the Schottky characteristics. For dry etching of GaN/AlGaN heterostructure two types of gas chemistry are explored: (1) $Cl_2/BCl_3/N_2$ and (2) Cl_2/Ar. It is observed that the first recipe gives very high etch rate which is a function of the RF bias, however, the etching is non-selective. The experimentally determined etch-rate as a function of a RF bias is shown in Fig. 4.6. This recipe is suitable for mesa etching, which requires deep anisotropic etching independent of the GaN/AlGaN material.

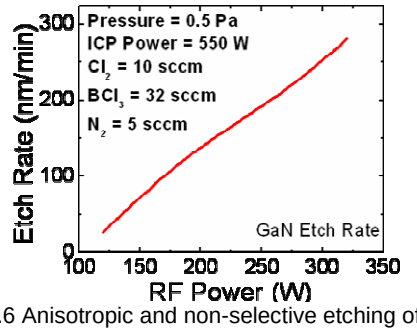

Fig. 4.6 Anisotropic and non-selective etching of GaN.

The recess etching requires much more selectivity and controllability. It is observed that Ar/Cl recipe gives a much smaller and controlled etch rate and 1:9 selectivity between GaN and AlGaN. The selectivity as a function of Ar flow rate is shown in Fig. 4.7. The highly selective and anisotropic (as shown in inset to Fig. 4.7) characteristics makes it suitable for gate and source/drain recess etching. A micro-photograph of the complete device as fabricated using the calibrated processes is shown in Fig. 4.8. Devices with two channel lengths and 100 μm width are fabricated. It is to be noted that the gate contact is deliberately tapered for easy lift-off the gate metal. The minimum channel

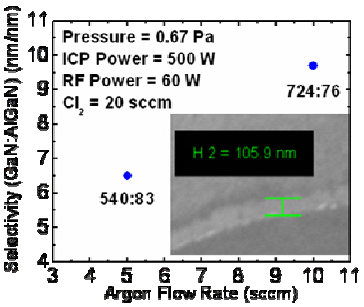

Fig. 4.7 Selective and controlled etching of GaN and AlGaN.

length of the device is kept at 2 μm. The DC characteristics of the devices are

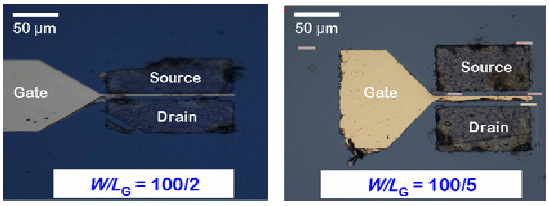

Fig. 4.8 Micro-photographs of HEMTs.

measured in a probe station and using appropriate sources and meters. The output characteristics of the device are shown in Fig. 4.9. The devices show clear sign of saturation. However, the degree of saturation is less for higher gate voltages

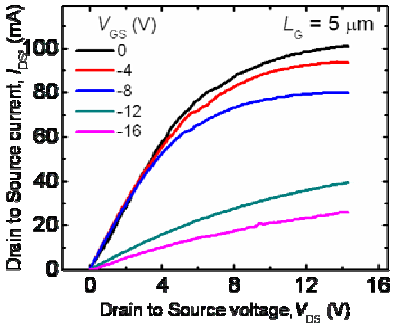

Fig. 4.9 Output characteristics of the HEMT.

because of larger leakage current. The transfer characteristic [Fig. 4.10(a)] is also measured to extract the transistor parameters. The threshold voltage is extracted by plotting the square root of the drain-to-source (I_{DS}) current versus gate to source (V_{GS}) voltage as shown in Fig. 4.10 (b). A peak transconductance of 130 mS/mm is measured for V_{GS} = -13V. The threshold voltage of the device is found to be V_{TH} = -25V.

4.5 Status and Future Work

The basic GaN HEMT device is demonstrated here. All the processing steps for fabrication are also characterized. The progress on GaN devices has been continuous and on-time. The device geometry (T-gate, field plate, degree of gate recession etc.) is being

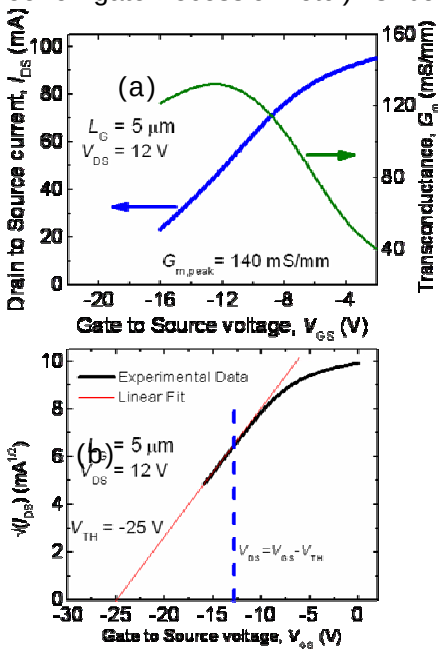

Fig. 4.10 (a) Transfer characteristics and transconductance of the device; (b) threshold voltage extraction.

optimized now and the optimum heterostructure (GaN/AlGaN heterostructure barrier and InGaN barrier for 2DEG confinement [3]) for the best performance is also being explored.

4.6 Other Work

4.6.1 InAs/GaAs Multi-Layer Quantum dot

Self assembled InAs/GaAs quantum dots have attracted increasing interest owing to their optoelectronic device application like in photodetectors, lasers etc. The efficiency, high temperature stability and high speed of QD devices strongly depends upon the dot density, size of the dots, uniformity in dot-size distribution and coherency of the dots. We have investigated the optical and structural properties of self assembled InAs/GaAs quantum dots (QDs) heterosturcture, single layer, bi-layer and multilayer format in great details by means of PL, AFM, HRTEM, HRXRD and Raman measurements. The important aspects of research in BQD system are the vertical ordering (stacking) and electronic coupling

between the adjacent QD layers. The significance of multilayer QD structure is to achieve greater active volume than that of a single layer system enhancing the gain and sensitivity of such devices. After investigating characterization part we fabricated IR detector using lithography, metallization and wet etching technique.

A schematic of the heterostructure grown by MBE is shown in Fig. 4.11. An SEM

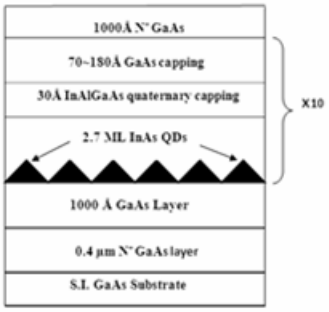

Fig. 4.11 A schematic of the IR photo-detector.

image of the strain-coupled multi-layer quantum dot is shown in Fig. 4.12. An increase in size of the dots from around 20nm in the bottom layer to 35-38nm in

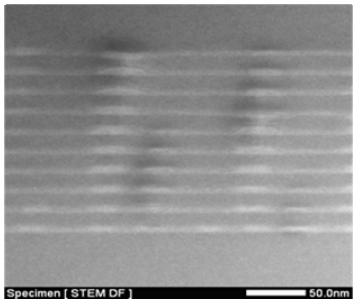

Fig. 4.12 Strained coupled multi-layer quantum dot.

the upper layers was observed. Teashick capping upon dot layer caused nice stacking of dots. A micro-photograph of the fabricated photodiode is shown in Fig. 4.13. The devices are being characterized to determine the IR response. Room

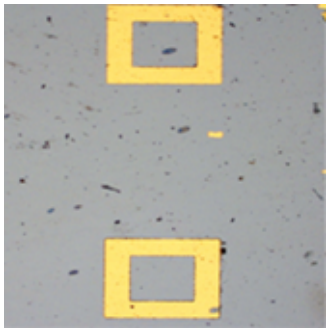

Fig. 4.13. A micro-photograph of the IR photodetector.

temperature *I-V* shows promising response.

4.6.2 c-Oriented GaN nanopillars formed by dry etching

Growth of semiconductor nanowires (pillars/whiskers) has gained considerable interests worldwide due to their potential for application in quantum electronics, optoelectronics, biosensors *etc*[4,5]. Already, there are reports of achieving sophisticated device structures such as field effect transistors, biosensors and even logic gates based on semiconductor nanowires[6]. However, many fundamental questions about the role of surface states on the transport and optical properties of these nanostructures remains unanswered till today. Here, we report the fabrication of highly oriented GaN nanopillars by etching GaN thin film using Inductively Coupled Plasma Reactive Ion Etching (ICP-RIE) technique (top-down approach). The GaN samples, used in this study, were purchased from TDI corp. of USA. These samples were grown on c-plane sapphire using HVPE growth technique. SENTECH SI 500 system was used for etching. ICP power used for etching was varied from 300-500 watts in steps of 50 watts. The RF power was fixed at 325 watts. Chlorine chemistry (Cl_2/Ar) was used to perform the etching.

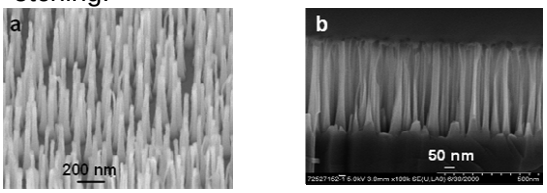

Fig. 4.14 (a) SEM image taken at an angle of 45° of the surface of the GaN layer after ICPRIE etching. An assembly of oriented GaN nanopillars is clearly visible. (b) Cross-sectional SEM image of the same sample.

Figure 1 shows the SEM images of the (a) surface and the (b) cross-section of the GaN layer after the etching. Formation of highly oriented vase-shaped nanopillars of GaN can be seen. The average diameter of these nanopillars is about 50 nm and their height is almost uniform. The height can be controlled by varying the etching

time. The density of these pillars is found to be a function of the ICP power. It has been found that the density as high as 2×10^{10} cm^{-2} can be obtained by optimizing the ICP power.

Figure 2 compares the photoluminescence (PL) spectra taken on the GaN bulk (black line) and the nanopillars (red line). In order to separate the nanopillars from the GaN base part the etched sample is dipped in methanol and kept in ultrasonic bath for 20 minutes. PL is done on the nanopillars after drop-casting methanol solution on a Si surface. While a strong blue luminescence (BL) band dominates the bulk PL spectrum, it is quite weak in nanopillars. On the other hand, a broad green luminescence (GL) band can be seen in the PL spectrum of the nanopillars, which is absent in the bulk spectrum. While in case of bulk, the neutral donor bound (D^oX) excitonic transition could be seen as a dominant feature at the band edge, in case of nanopillars, a sharp defect bound excitonic (Y2) feature dominates the band edge. Many other defect related transitions, which are typically known as Y_i transitions in GaN[7], could be seen in the PL spectrum of the nanopillars (Inset of Fig. 2). Note that Y_i transitions are mostly absent in our state of the art bulk GaN layers. The dominance of the defect related transitions in the PL spectrum of the nanopillars must be due to the increased surface to volume ratio in these structures

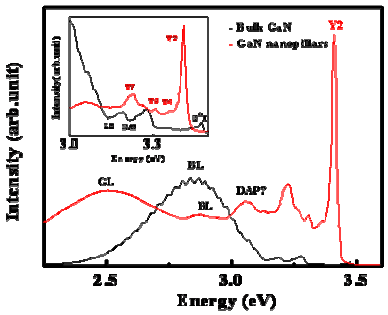

Fig. 4.15 PL spectra taken at 10K on the GaN bulk (black line) and the nanopillars (red line). Inset compares the two spectra near to the band edge.

Here, we believe that the selective etching of the N-polar inversion domains between Ga-polar domains by the Chlorine plasma results in the formation of nanopillars. Inversion domain boundaries (IDB) in the molecular beam epitaxy (MBE) and HVPE grown samples are found to extend from the bottom to the top of the layer and formed columnar domains with width up to 100 nm in HVPE grown samples[8].

4.7 References:

[1] C. Q. Chen *et. al.*, "AlGaN/GaN/AlGaN double heterostructure for high-power III-N field-effect transistors," *Appl. Phys. Lett.*, vol.82, p. 4593 (2003).

[2] N. Maeda *et. al.*, "Enhanced effect of polarization properties in AlGaN/GaN double-heterostructure field-effect transistors", *Appl. Phys. Lett.*, vol. 76, p.

[3] T. Palacois *et. al.*, "AlGaN/GaN high electron mobility transistors with InGaN back-barriers", *IEEE Elec. Dev. Lett.*, vol. 27, p. 13 (2006).

[4] L. Lauhon *et al.,* "Epitaxial core–shell and core–multishell nanowire heterostructures", *Nature*, vol. 420, p. 57 (2002).

[5] M. Gudiksen *et al.,* "Growth of nanowire superlattice structures for nanoscale photonics and electronics", *Nature* vol. 415, p. 617 (2002).

[6] A. Greytak *et al.,* "Growth and transport properties of complementary germanium nanowire field-effect transistors", *Appl. Phys. Lett.,* vol. 84, p. 4176 (2004).

[7] A. Michael *et al.,* "Luminescence properties of defects in GaN", *J. Appl. Phys.*, vol. 97, p. 061301 (2005).

[8] L. T. Romano *et al.,* "Inversion domains in GaN grown on sapphire", *Appl. Phys. Letts.,* Vol. 69, p. 2394 (1996).